Supplementary Materials

for

"G3BP1 Binds to Guanine Quadruplexes in mRNAs to Modulate Their Stabilities"

Xiaomei He, Jun Yuan and Yinsheng Wang*

Department of Chemistry, University of California Riverside, CA 92521-0403, USA

*To whom correspondence should be addressed: yinsheng.wang@ucr.edu

Table of Contents

Table S1. Summary of overlapping percentages between eCLIP-seq data (1) and rG4-seq data (GSE77282_KPDS_hits) (2). Some known rG4 binding proteins are highlighted in blue.

File accessions	Experiment Targets	Cell Lines	Total Peaks	Overlapping Peaks (*P*< 0.05)	Overlapping Percentages
ENCFF575BCP	AKAP1	HepG2	5878	4047	68.9%
ENCFF727XDH	DDX55	K562	1114	749	67.2%
ENCFF814JGE	UPF1	K562	13450	9015	67.0%
ENCFF153CMF	CPEB4	K562	194	130	67.0%
ENCFF242FDW	UPF1	HepG2	9600	6359	66.2%
ENCFF545FMX	NPM1	K562	41	26	63.4%
ENCFF901ABJ	SUPV3L1	K562	40	25	62.5%
ENCFF846JEW	DDX6	K562	1992	1217	61.1%
ENCFF822NMS	DDX55	HepG2	1746	1028	58.9%
ENCFF982RHC	RBM15	HepG2	1519	882	58.1%
ENCFF975HKC	PABPN1	HepG2	3955	2296	58.1%
ENCFF368MXJ	FAM120A	K562	5681	3249	57.2%
ENCFF103XLC	GRSF1	HepG2	994	568	57.1%
ENCFF470JIH	PUS1	K562	7	4	57.1%
ENCFF241KPE	SDAD1	K562	43	24	55.8%
ENCFF982GEG	ZRANB2	K562	368	202	54.9%
ENCFF736YDH	APOBEC3C	K562	990	541	54.7%
ENCFF358QSY	WDR43	K562	135	73	54.1%
ENCFF756RYJ	AARS	K562	36	19	52.8%
ENCFF327WXM	ZC3H11A	K562	1245	656	52.7%
ENCFF565BTR	METAP2	K562	3067	1616	52.7%
ENCFF431FMQ	PCBP1	K562	2194	1152	52.5%
ENCFF956PEQ	PABPC4	K562	5915	3051	51.6%
ENCFF481RZR	NCBP2	K562	412	209	50.7%
ENCFF367VYJ	DDX42	K562	107	54	50.5%
ENCFF700XBC	FMR1	K562	3072	1549	50.4%
ENCFF363IJZ	FXR2	K562	3994	2013	50.4%
ENCFF263BIJ	LARP4	HepG2	5679	2846	50.1%
ENCFF788UFQ	SRSF1	K562	2155	1074	49.8%
ENCFF637JMJ	LSM11	HepG2	2429	1196	49.2%
ENCFF963CVD	G3BP1	HepG2	6541	3210	49.1%
ENCFF758EWI	SUPV3L1	HepG2	214	105	49.1%
ENCFF108TOJ	PCBP1	HepG2	960	467	48.7%

File accessions	Experiment Targets	Cell Lines	Total Peaks	Overlapping Peaks (*P*< 0.05)	Overlapping Percentages
ENCFF190WAS	EFTUD2	K562	5635	2733	48.5%
ENCFF431WWR	WDR43	HepG2	196	95	48.5%
ENCFF324PNB	SSB	K562	163	79	48.5%
ENCFF261SMW	DDX6	HepG2	548	265	48.4%
ENCFF969AOQ	PUM1	K562	2620	1265	48.3%
ENCFF097FBP	SF3B4	HepG2	5843	2814	48.2%
ENCFF527BMM	RBM15	K562	9282	4453	48.0%
ENCFF640DDA	TIA1	HepG2	1704	817	48.0%
ENCFF017IRY	EFTUD2	HepG2	7850	3756	47.9%
ENCFF530MIN	SRSF1	HepG2	1781	838	47.1%
ENCFF055TAZ	ZC3H11A	HepG2	1156	543	47.0%
ENCFF310NDD	FXR1	K562	1376	642	46.7%
ENCFF727HMM	SERBP1	K562	140	65	46.4%
ENCFF977MKB	IGF2BP2	K562	3819	1771	46.4%
ENCFF331VCF	SND1	K562	4118	1907	46.3%
ENCFF004IIT	TRA2A	K562	1731	801	46.3%
ENCFF710LWM	SF3A3	HepG2	2524	1154	45.7%
ENCFF449ZHX	SRSF7	K562	479	218	45.5%
ENCFF834BGX	RPS3	K562	2393	1089	45.5%
ENCFF080PGT	BUD13	HepG2	4244	1930	45.5%
ENCFF598NYT	FUBP3	HepG2	2787	1262	45.3%
ENCFF400KYS	AQR	K562	25937	11728	45.2%
ENCFF767LWE	PUM2	K562	5661	2555	45.1%
ENCFF565RQI	SSB	HepG2	91	41	45.1%
ENCFF540UOQ	LIN28B	K562	6778	3050	45.0%
ENCFF207UUG	ZC3H8	K562	258	116	45.0%
ENCFF851FUY	XRN2	K562	1510	678	44.9%
ENCFF187VMX	SF3B4	K562	10684	4770	44.7%
ENCFF351RHN	AQR	HepG2	11300	5042	44.6%
ENCFF651CNX	BUD13	K562	8386	3738	44.6%
ENCFF917NGY	TRA2A	HepG2	947	421	44.5%
ENCFF311TOZ	IGF2BP3	HepG2	2189	965	44.1%
ENCFF264WFT	CPSF6	K562	755	332	44.0%
ENCFF929AVT	ABCF1	K562	57	25	43.9%
ENCFF875QBF	GEMIN5	K562	2636	1154	43.8%
ENCFF510KUY	SUB1	HepG2	3405	1489	43.7%
ENCFF579NNP	ZNF800	K562	2411	1049	43.5%

File accessions	Experiment Targets	Cell Lines	Total Peaks	Overlapping Peaks (*P*< 0.05)	Overlapping Percentages
ENCFF985DTC	RPS3	HepG2	5861	2532	43.2%
ENCFF284NOU	LARP4	K562	434	187	43.1%
ENCFF034YUT	FTO	HepG2	567	244	43.0%
ENCFF865SCT	PRPF8	HepG2	20051	8578	42.8%
ENCFF284MRX	PPIG	HepG2	22811	9668	42.4%
ENCFF441YAZ	FTO	K562	853	360	42.2%
ENCFF146YIO	GRWD1	K562	4293	1803	42.0%
ENCFF451AQL	LIN28B	HepG2	3829	1608	42.0%
ENCFF792WPY	DDX24	K562	9615	4030	41.9%
ENCFF885OWJ	DDX3X	HepG2	8913	3707	41.6%
ENCFF667MXK	DDX3X	K562	6891	2854	41.4%
ENCFF357ABQ	FASTKD2	K562	553	229	41.4%
ENCFF322GPD	SF3B1	K562	29	12	41.4%
ENCFF391KVJ	UCHL5	HepG2	2104	869	41.3%
ENCFF485KCC	PRPF4	HepG2	9237	3790	41.0%
ENCFF374PBK	UCHL5	K562	17995	7375	41.0%
ENCFF400CFS	RBM5	HepG2	589	241	40.9%
ENCFF534ONM	EIF3G	K562	289	117	40.5%
ENCFF146YPF	DDX51	K562	450	182	40.4%
ENCFF329VBT	XRCC6	K562	847	342	40.4%
ENCFF933AGU	RBM22	HepG2	1876	756	40.3%
ENCFF693EMF	SMNDC1	HepG2	355	143	40.3%
ENCFF582WWR	RBFOX2	K562	3462	1393	40.2%
ENCFF047PZR	NOL12	HepG2	266	107	40.2%
ENCFF304YLR	TBRG4	HepG2	15	6	40.0%
ENCFF567MGK	YBX3	K562	18356	7318	39.9%
ENCFF119DHE	SMNDC1	K562	2517	1002	39.8%
ENCFF387ZAH	TIAL1	HepG2	2432	965	39.7%
ENCFF239WCW	DGCR8	K562	1238	490	39.6%
ENCFF149CJJ	FXR2	HepG2	3935	1550	39.4%
ENCFF101EKG	SND1	HepG2	6988	2750	39.4%
ENCFF928OEC	EIF3H	HepG2	2908	1141	39.2%
ENCFF242WEP	DGCR8	HepG2	1662	650	39.1%
ENCFF890VLH	IGF2BP1	K562	5617	2192	39.0%
ENCFF448SCQ	HNRNPK	K562	3026	1179	39.0%
ENCFF021VWK	U2AF1	HepG2	1034	400	38.7%
ENCFF298ZAG	TIA1	K562	5811	2246	38.7%

File accessions	Experiment Targets	Cell Lines	Total Peaks	Overlapping Peaks (*P*< 0.05)	Overlapping Percentages
ENCFF092XHF	NIPBL	K562	316	121	38.3%
ENCFF238REI	DROSHA	K562	3898	1492	38.3%
ENCFF517ECT	IGF2BP1	HepG2	4443	1696	38.2%
ENCFF151HRC	NOLC1	K562	1549	591	38.2%
ENCFF949RPR	PRPF8	K562	10956	4175	38.1%
ENCFF456PLF	NCBP2	HepG2	3234	1230	38.0%
ENCFF713QGM	GRWD1	HepG2	21551	8122	37.7%
ENCFF546ZFM	MTPAP	K562	982	368	37.5%
ENCFF955PCQ	HNRNPA1	K562	166	62	37.4%
ENCFF456SOS	UTP18	K562	134	50	37.3%
ENCFF800XSC	GNL3	K562	27	10	37.0%
ENCFF163SWW	U2AF1	K562	1230	451	36.7%
ENCFF514KIW	AATF	K562	1078	395	36.6%
ENCFF265RIO	FASTKD2	HepG2	877	320	36.5%
ENCFF445JRX	GTF2F1	K562	4976	1814	36.5%
ENCFF958EFT	PHF6	K562	678	246	36.3%
ENCFF509AKB	TBRG4	K562	315	112	35.6%
ENCFF154DRN	RBFOX2	HepG2	7337	2602	35.5%
ENCFF538ZHY	LSM11	K562	1323	460	34.8%
ENCFF560CDL	PCBP2	HepG2	8698	3022	34.7%
ENCFF889CCS	GPKOW	K562	1140	396	34.7%
ENCFF037BNT	ZNF622	K562	14936	5149	34.5%
ENCFF039FGP	RBM22	K562	1040	357	34.3%
ENCFF821EXR	HNRNPUL1	K562	202	69	34.2%
ENCFF717EQF	XRN2	HepG2	1664	561	33.7%
ENCFF938JQE	WRN	K562	119	40	33.6%
ENCFF105PMR	SBDS	K562	9	3	33.3%
ENCFF832JDM	UTP3	K562	18	6	33.3%
ENCFF331AFC	U2AF2	K562	3645	1208	33.1%
ENCFF159HMF	HNRNPC	K562	557	183	32.9%
ENCFF923ZLX	AKAP8L	K562	2104	690	32.8%
ENCFF741FRL	FAM120A	HepG2	8081	2648	32.8%
ENCFF944ISN	NOLC1	HepG2	1368	448	32.8%
ENCFF075NSB	SRSF9	HepG2	678	221	32.6%
ENCFF241SUC	GTF2F1	HepG2	4575	1491	32.6%
ENCFF131ZWK	TAF15	K562	561	180	32.1%
ENCFF623DVN	HLTF	K562	138	44	31.9%

File accessions	Experiment Targets	Cell Lines	Total Peaks	Overlapping Peaks (*P*< 0.05)	Overlapping Percentages
ENCFF355WVE	HNRNPUL1	HepG2	468	149	31.8%
ENCFF002FLD	DKC1	HepG2	2662	846	31.8%
ENCFF121XLA	HNRNPA1	HepG2	89	28	31.5%
ENCFF624RZR	DROSHA	HepG2	2105	662	31.5%
ENCFF546EKR	PPIL4	K562	643	201	31.3%
ENCFF777FHS	FUS	K562	4306	1346	31.3%
ENCFF793EJK	ZNF800	HepG2	2883	882	30.6%
ENCFF536BUW	CSTF2T	K562	10769	3273	30.4%
ENCFF074EQM	DDX59	HepG2	3070	928	30.2%
ENCFF485NXM	DHX30	K562	883	264	29.9%
ENCFF844VZT	HNRNPU	K562	188	56	29.8%
ENCFF865AZP	SRSF7	HepG2	438	130	29.7%
ENCFF374GKD	FKBP4	HepG2	1472	436	29.6%
ENCFF993NVI	HNRNPK	HepG2	5729	1687	29.5%
ENCFF800GPC	DDX21	K562	75	22	29.3%
ENCFF888SME	DDX52	K562	1274	361	28.3%
ENCFF842EFT	BCCIP	HepG2	508	142	28.0%
ENCFF061DTB	NKRF	HepG2	3804	1063	27.9%
ENCFF837ZOX	SLTM	HepG2	1318	366	27.8%
ENCFF159VOF	U2AF2	HepG2	10559	2928	27.7%
ENCFF934PXE	SAFB	K562	506	140	27.7%
ENCFF215XPR	WDR3	K562	29	8	27.6%
ENCFF204UQL	CDC40	HepG2	1215	335	27.6%
ENCFF877QKG	TROVE2	HepG2	164	45	27.4%
ENCFF656IDO	XRCC6	HepG2	95	26	27.4%
ENCFF955VYD	NIP7	HepG2	287	77	26.8%
ENCFF130JJX	EIF3D	HepG2	791	212	26.8%
ENCFF648LCX	EIF4G2	K562	4591	1198	26.1%
ENCFF257KKQ	DDX52	HepG2	132	34	25.8%
ENCFF075XTM	SDAD1	HepG2	860	221	25.7%
ENCFF363FKB	YWHAG	K562	777	199	25.6%
ENCFF259NLI	TARDBP	K562	6822	1741	25.5%
ENCFF890NIT	EWSR1	K562	8803	2208	25.1%
ENCFF075TIW	YBX3	HepG2	2116	529	25.0%
ENCFF363HHT	NONO	K562	11435	2855	25.0%
ENCFF693ZAZ	SLTM	K562	3544	878	24.8%
ENCFF440FET	XPO5	HepG2	4777	1181	24.7%

File accessions	Experiment Targets	Cell Lines	Total Peaks	Overlapping Peaks (*P*< 0.05)	Overlapping Percentages
ENCFF302FFF	LARP7	HepG2	246	60	24.4%
ENCFF469SRC	SAFB	HepG2	235	56	23.8%
ENCFF930HHV	BCLAF1	HepG2	32607	7697	23.6%
ENCFF514NWO	TROVE2	K562	487	114	23.4%
ENCFF336WDV	FUS	HepG2	789	182	23.1%
ENCFF305BNZ	LARP7	K562	260	59	22.7%
ENCFF945YRD	CSTF2T	HepG2	20334	4576	22.5%
ENCFF513PTZ	TAF15	HepG2	699	157	22.5%
ENCFF553APP	KHSRP	HepG2	5280	1179	22.3%
ENCFF937QJB	EXOSC5	HepG2	740	163	22.0%
ENCFF788LMZ	STAU2	HepG2	774	168	21.7%
ENCFF342PGS	HNRNPM	K562	6406	1372	21.4%
ENCFF222ULF	CSTF2	HepG2	2903	597	20.6%
ENCFF233ZXV	DHX30	HepG2	109	22	20.2%
ENCFF169SMQ	AGGF1	K562	4789	931	19.4%
ENCFF617LAH	AGGF1	HepG2	3744	706	18.9%
ENCFF370GDB	ILF3	K562	2931	548	18.7%
ENCFF871BYW	KHSRP	K562	22728	4149	18.3%
ENCFF485DDA	ILF3	HepG2	3228	583	18.1%
ENCFF105AKX	HNRNPC	HepG2	3144	560	17.8%
ENCFF410XHF	HLTF	HepG2	3515	624	17.8%
ENCFF924CZR	PTBP1	K562	7592	1341	17.7%
ENCFF027CBV	QKI	K562	2247	389	17.3%
ENCFF803GSP	RPS11	K562	24	4	16.7%
ENCFF170SCU	PTBP1	HepG2	8595	1408	16.4%
ENCFF296JHG	HNRNPL	K562	5683	906	15.9%
ENCFF926QBW	UTP18	HepG2	45	7	15.6%
ENCFF445CGF	QKI	HepG2	10367	1525	14.7%
ENCFF046VQV	MATR3	K562	5036	721	14.3%
ENCFF124YKO	KHDRBS1	K562	1255	179	14.3%
ENCFF036IYW	NSUN2	K562	155	22	14.2%
ENCFF890KEE	HNRNPL	HepG2	9010	1262	14.0%
ENCFF456CGG	SLBP	K562	154	21	13.6%
ENCFF878JOG	HNRNPM	HepG2	13251	1795	13.6%
ENCFF854NXI	HNRNPU	HepG2	285	36	12.6%
ENCFF805LKH	SFPQ	HepG2	2582	318	12.3%
ENCFF427AAU	EXOSC5	K562	12002	1450	12.1%

File accessions	Experiment Targets	Cell Lines	Total Peaks	Overlapping Peaks (*P*< 0.05)	Overlapping Percentages
ENCFF764MPF	SUGP2	HepG2	14644	1588	10.8%
ENCFF193UPY	SAFB2	K562	3699	396	10.7%
ENCFF298YFY	MATR3	HepG2	7168	740	10.3%
ENCFF014MZO	POLR2G	HepG2	51	5	9.8%

Table S2. Summary of previously published rG4 binding proteins.

Known rG4-binding Proteins	Ref.
DDX21	(3)
DDX1	(4)
DDX5	(5)
DDX3X	(1)
DHX9	(6)
DHX36	(7)
EIF4A	(8)
EWSR1	(9)
GRSF1	(10)
hnRNP H/F	(11)
hnRNPA1	(12)
hnRNPU	(13)
NCL	(14)
NONO	(15)
NSUN5	(1)
TFAM	(16)
YBX3	(17)
FMR1	(18)
FXR1	(19)
FXR2	(1)
CNBP	(20)
AVEN	(21)
SRSF1	(17)
SF3B2	(22)
EIF4G	(23)

Table S3. Oligonucleotides used in this study.

RNA G4 and mutated probes	
Sequence Names	Sequences
PITX1 rG4	5′-TAMRA-GAGCGGGGAAGGGCGCGGGCGCGGGCGCGG-3′
PITX1 rM4	5′-TAMRA-GAGCGCGGAAGCGCGCGCGCGCGCGCGG-3′
NRAS rG4	5′-Cy3-GUGUGGGAGGGGCGGGUCUGGGUGCG
NRAS rM4	5′-Cy3-GUGUAAAAGGGGCGGGUCUGGGUGCG
PITX1 rG4	5′-Biotin-TTTGAGCGGGGAAGGGCGCGGGCGCGGGCGCGG-3′
PITX1 rM4	5′-Biotin-TTTGAGCGCGGAAGCGCGCGCGCGCGCGCGG-3′
Sequence used for CRISPR/Cas9 editing	
Sequence Names	Sequences
sgRNA	5′-AAATTCCCGCCCGACCAGCA-3′
Primers used for RT-qPCR	
Sequence Names	Sequences
GAPDH-F	5′-TTCGACAGTCAGCCGCATCTTCTT-3′
GAPDH-R	5′-CAGGCGCCCAATACGACCAAATC-3′
PITX1-F	5′-GACCCAGCCAAGAAGAAGAA-3′
PITX1-R	5′-GCCCAGTTGTTGTAGGAGTAG-3′
KHSRP-F	5′-GAATGAGTACGGATCTCGGATTG-3′
KHSRP-R	5′-CTCCCGTCTGCTGGTTTATG-3′
ACTR2-F	5′-AGCTTTGGTTGGAAGACCTATTA-3′
ACTR2-R	5′-CTGCCTGGATGGCTACATATAC3′
Firefly-F	5′-CCAGGTATCAGGCAAGGATATG-3′
Firefly-R	5′-GTTCGTCTTCGTCCCAGTAAG-3′
Renilla-F	5′-GCAGAAGTTGGTCGTGAGG-3′
Renilla-R	5′-TCATCCGTTTCCTTTGTTCTG-3′

Figure S1. Integrative Genomics Viewer (IGV) plots showing representative comparison results of rG4-seq data with AKAP1 eCLIP-seq data (A-B) and MATR3 eCLIP-seq data (C-D).

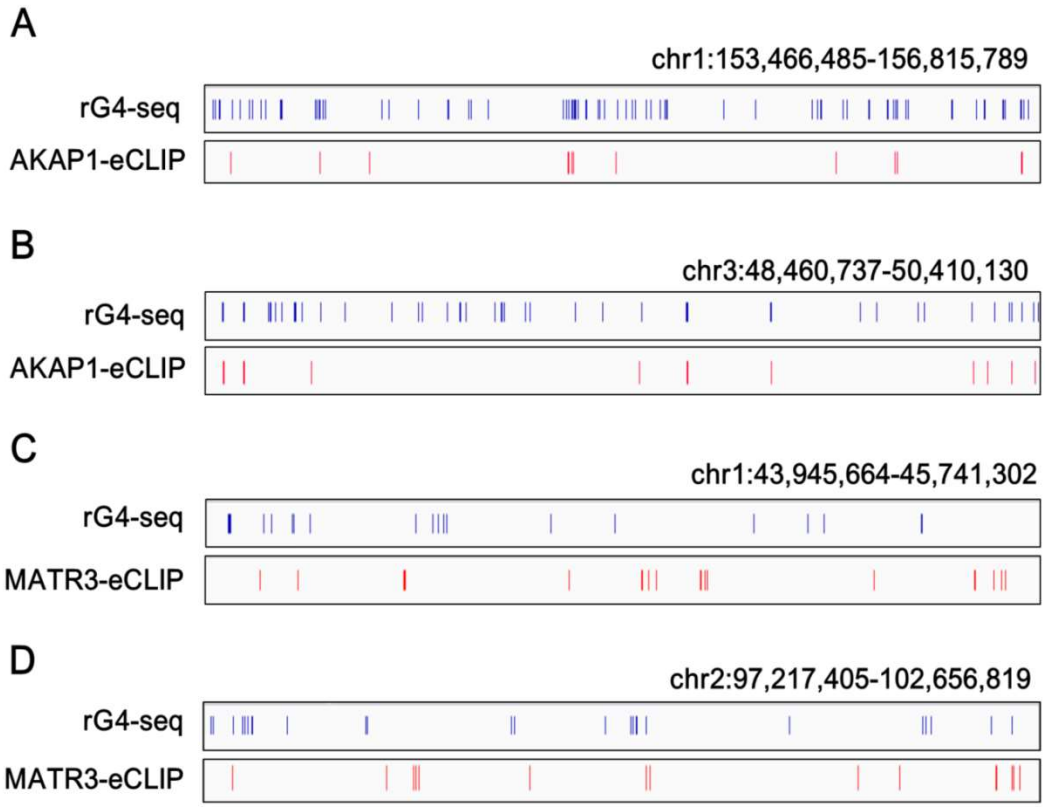

Figure S2. Overlap of known rG4-binding proteins between RNA-binding proteins identified in this study and previously published rG4-binding proteins.

Figure S3. Integrative Genomics Viewer (IGV) plots showing putative G4 forming sequences in the overlapping regions between G3BP1 eCLIP-seq peaks and rG4-seq peaks. Representative overlapping regions located in the mRNAs of (A) *LRP5* and (B) *FADS2* genes.

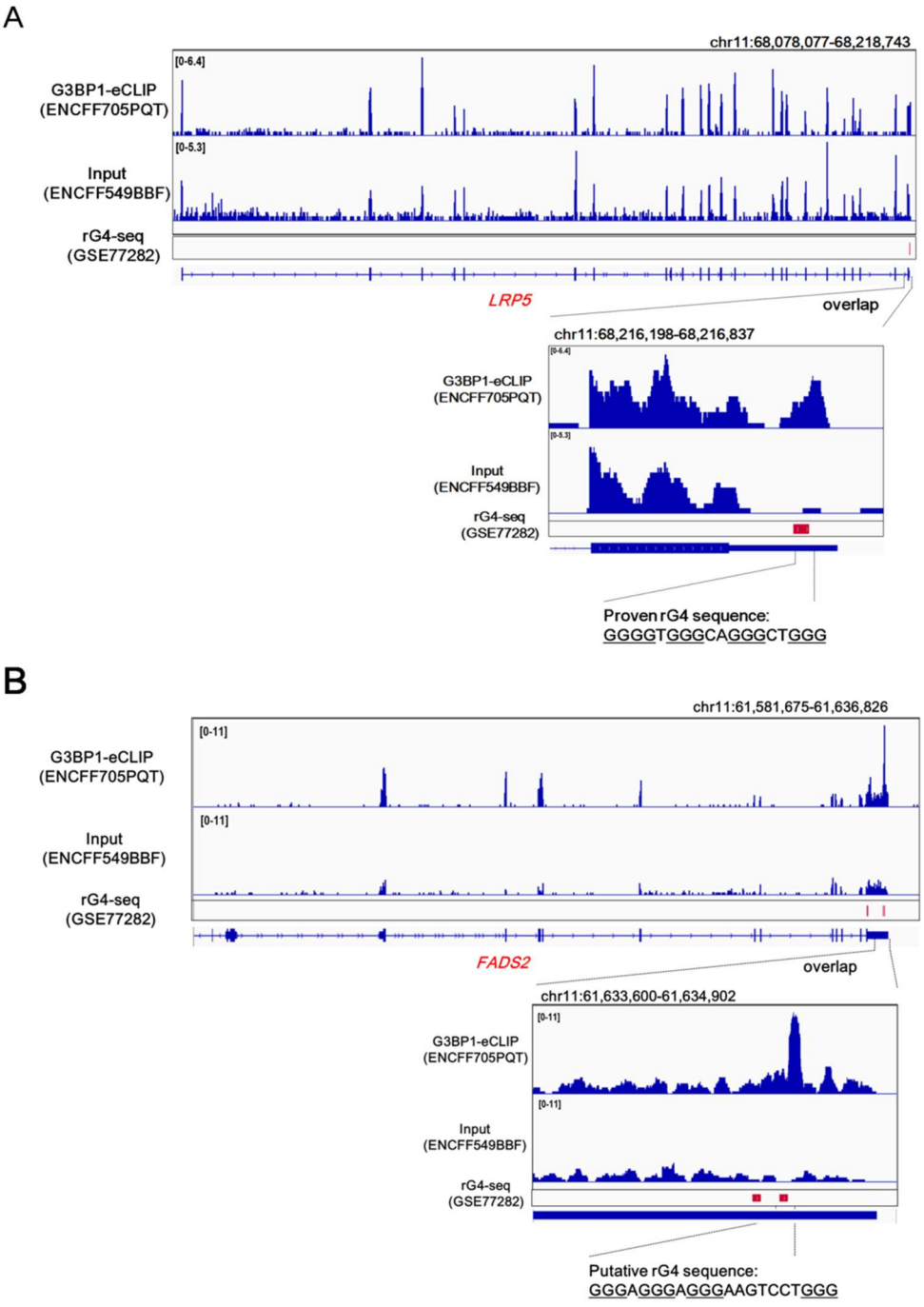

Figure S4. SDS-PAGE gel of GST-G3BP1 protein and its four truncated variants.

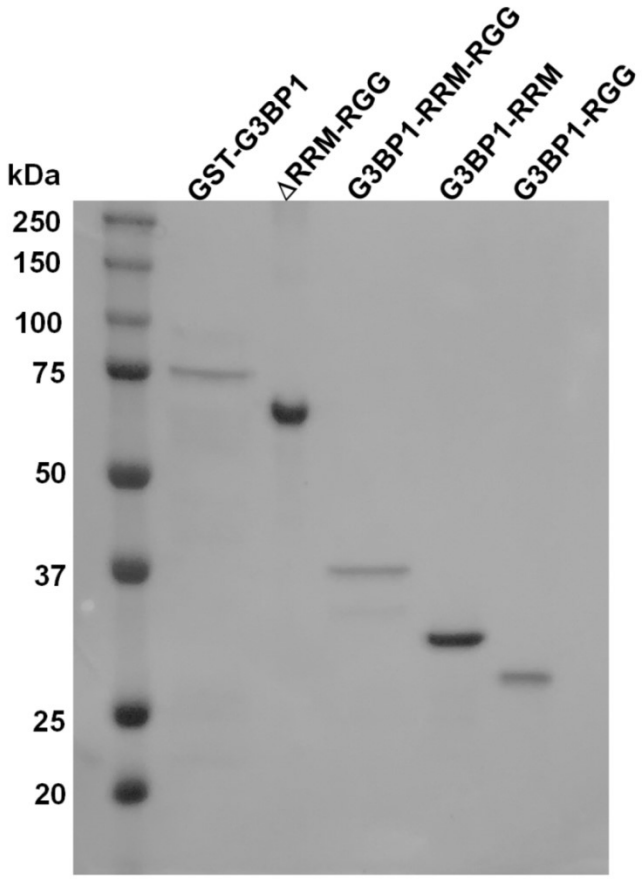

Figure S5. Circular dichroism (CD) spectra of PITX1 rG4 (A), NRAS rG4 (B), PITX1 rG4 in the presence of G3BP1 protein (C), and G3BP1 protein only (D). The CD spectrum of rG4 in the G3BP1-rG4 complex (C) was obtained by subtracting the CD spectrum of G3BP1 protein (D) from CD spectrum of the mixture (no shown).

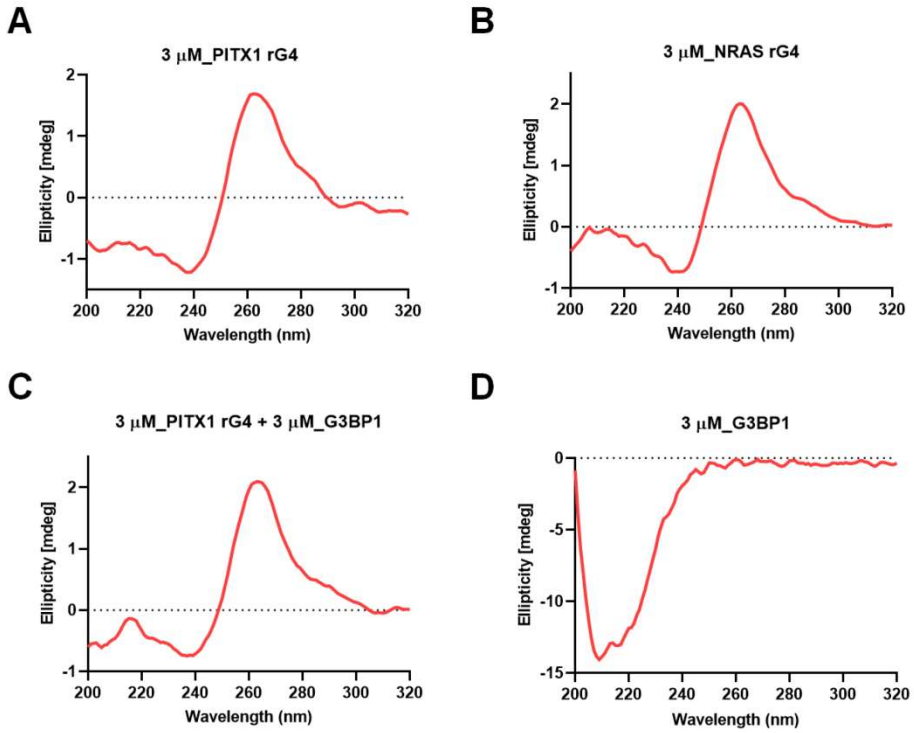

Figure S6. EMSA for monitoring the G3BP1-rG4 interaction with increasing concentrations of G3BP1 (A), and with a fixed concentration of G3BP1 together with increasing concentrations of PDS (B).

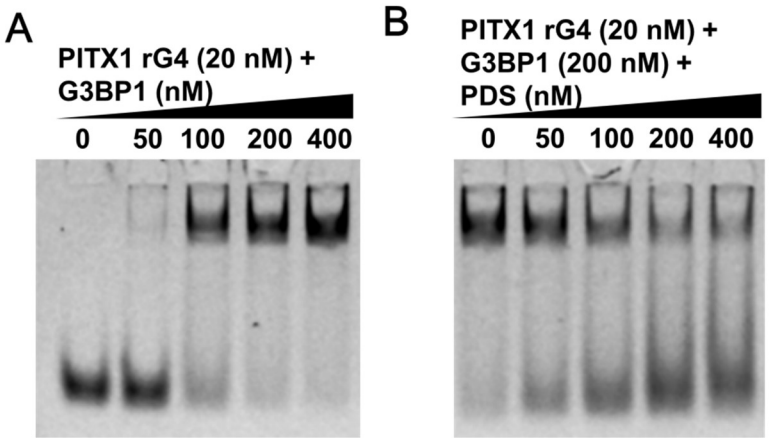

Figure S7. Representative Sanger sequencing results showing CRISPR-induced indel mutations of *G3BP1* gene in HEK293T cells (A) and HeLa cells (B) (i.e., *G3BP1*$^{-/-}$ cells).

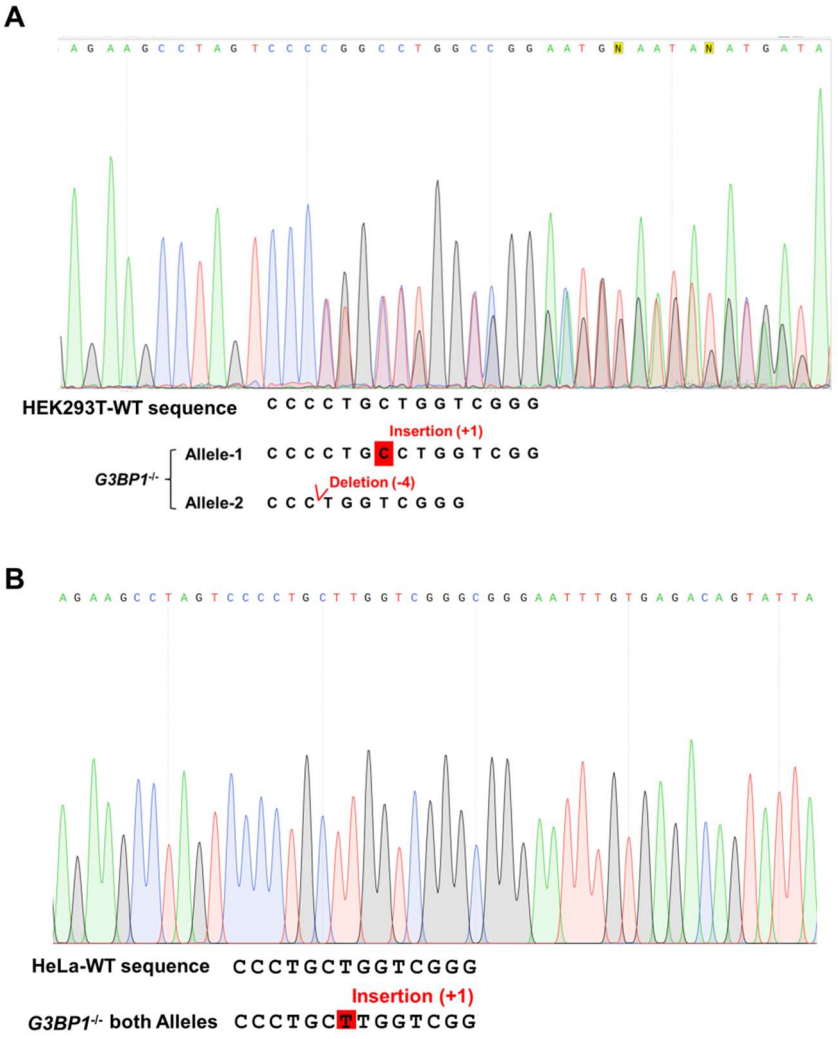

F

Figure S8. RT-qPCR and Western blot showing the mRNA and protein levels of Flag-PITX1 in HEK293T cells and the isogenic *G3BP1*$^{-/-}$ cells. (A-C) A comparison of the mRNA and protein expression levels of Flag-PITX1 in HEK293T cells transfected with Flag-PITX1-WT or Flag-PITX1-3Qm plasmid. (D-F) A comparison of the mRNA and protein expression levels of Flag-PITX1 in *G3BP1*$^{-/-}$ HEK293T cells transfected with Flag-PITX1-WT or Flag-PITX1-3Qm plasmid. Error bars represent S.E.M. (n = 3). The *p* values were calculated by using unpaired, two-tailed Student's *t*-test. ns, $p > 0.05$; **, $0.001 \leq p < 0.01$; ***, $p < 0.001$.

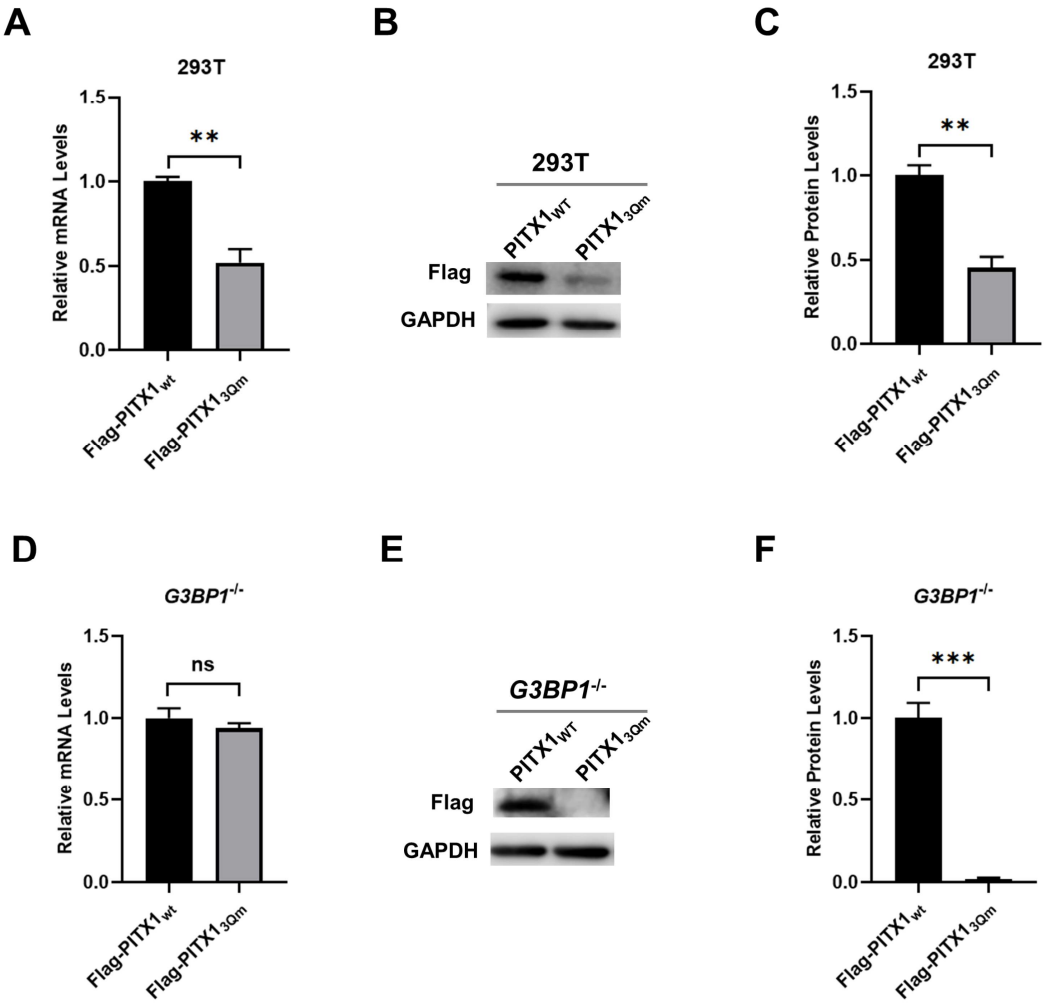

Figure S9. seCLIP-seq peaks annotation for “Ctrl” dataset (A) and “PDS” dataset (B).

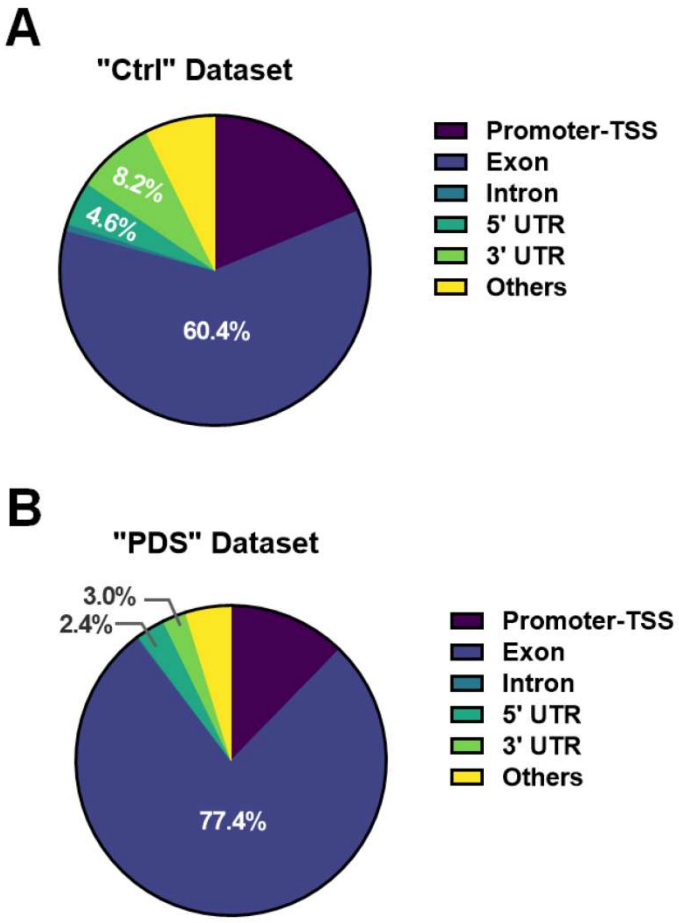

Figure S10. IGV plots showing the comparison of G3BP1 peaks from seCLIP-seq Replicate-1 (A) and Replicate-2 (B) around the rG4- forming sequences located in the 3′-UTR of *PITX1* gene between control (Ctrl) and PDS-treated (PDS) cells.

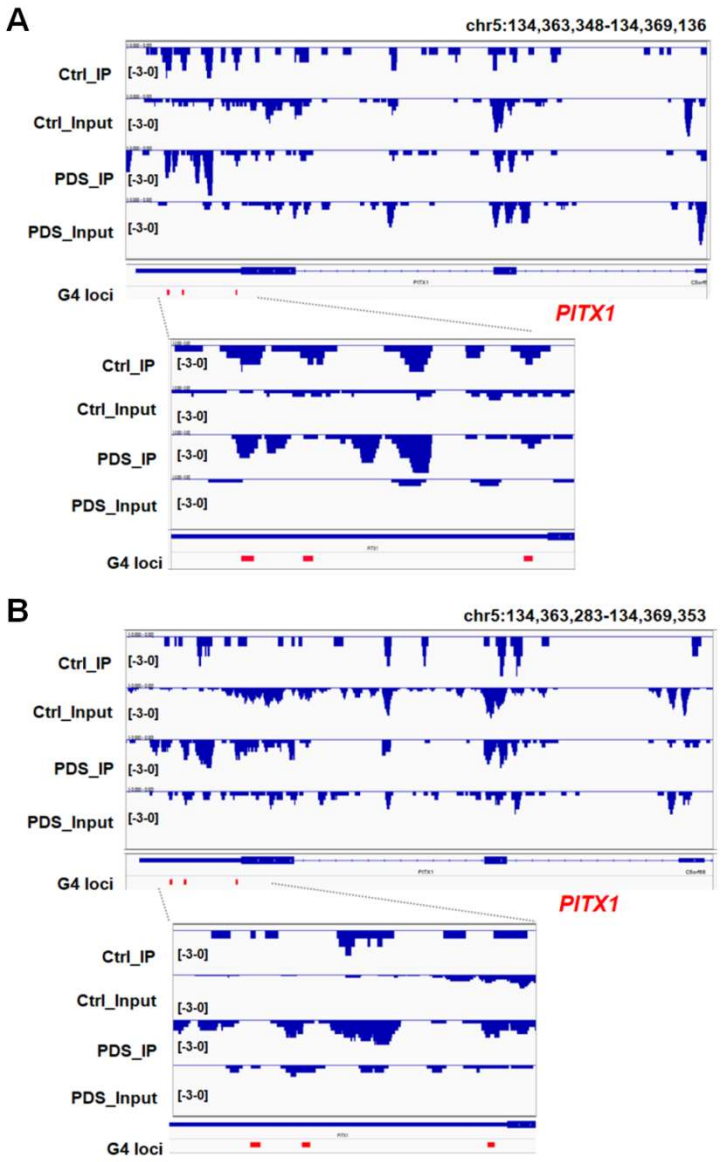

Figure S11. IGV plots showing the comparison between "Ctrl" and "PDS" peaks from seCLIP-seq Replicate-1 (A) and Replicate-2 (B) around the rG4-forming sequence located at 5′-UTR of *NRAS* gene.

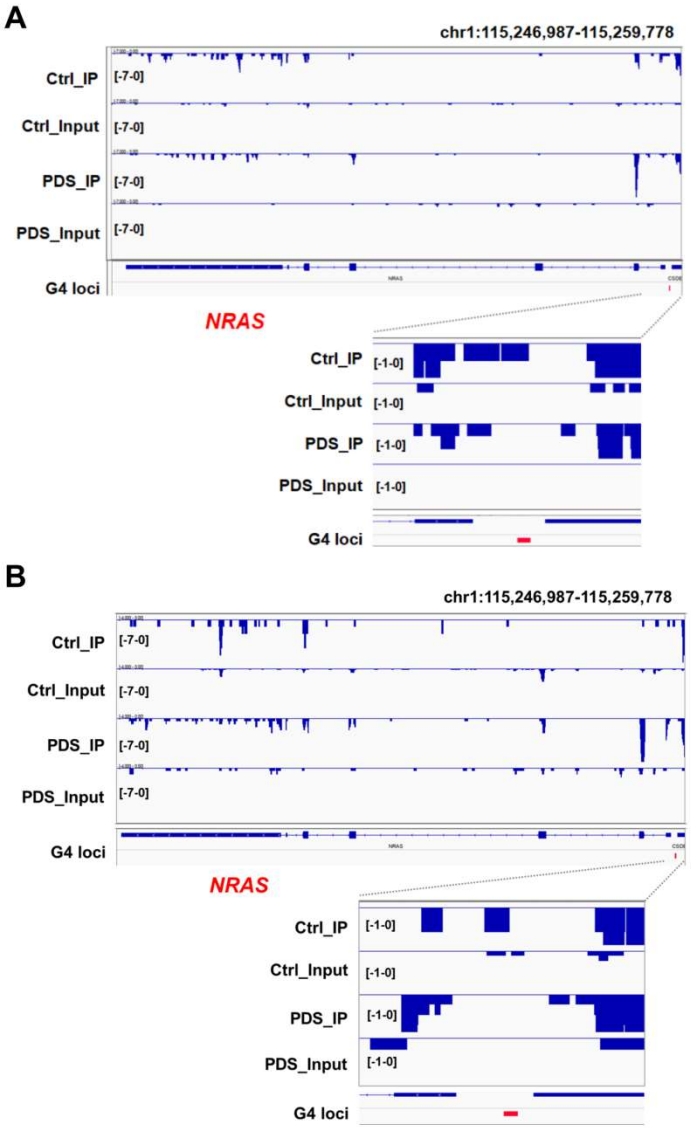

Figure S12. IGV plots showing the comparison between "Ctrl" and "PDS" peaks from seCLIP-seq Replicate-2 around the rG4-forming sequences located at 5′- and 3′-UTR of *KHSRP* gene.

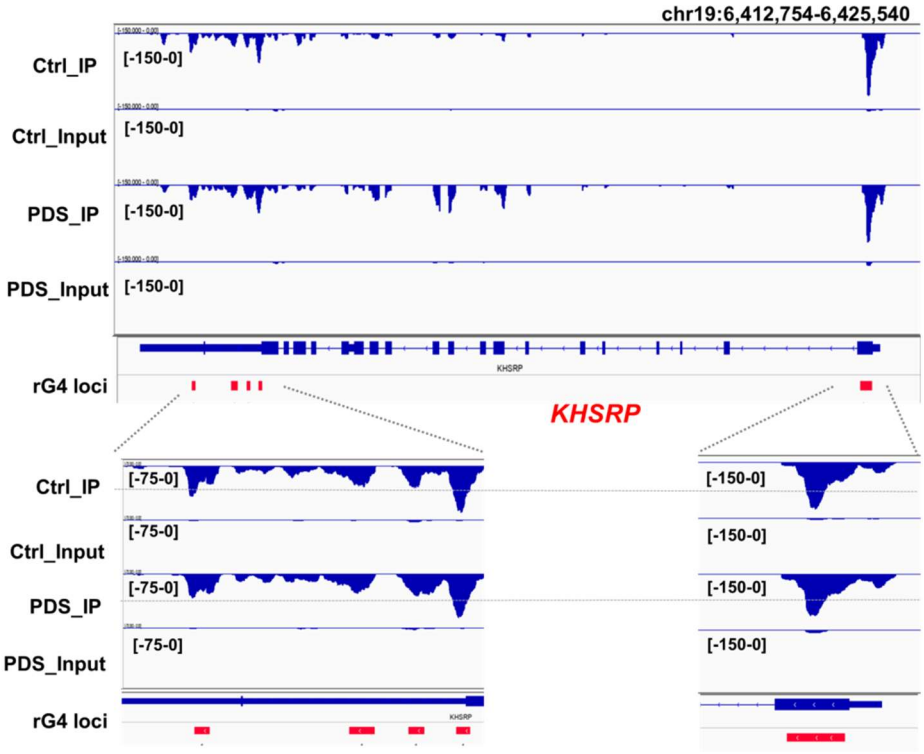

Figure S13. IGV plots showing the comparison between "Ctrl" and "PDS" peaks from seCLIP-seq Replicate-1 (A) and Replicate-2 (B) around the rG4-forming sequences located at 3′-UTR of *ACTR2* gene.

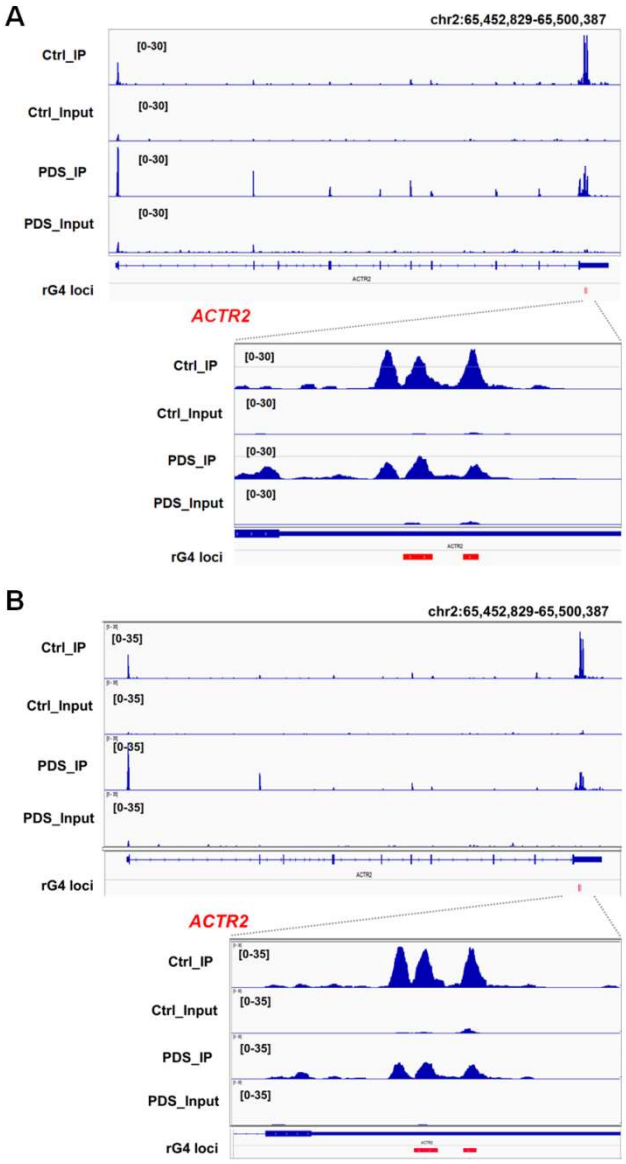

Figure S14. RT-qPCR results showing the half-lives of (A) KHSRP and (B) ACTR2 mRNAs in 293T cell, the isogenic *G3BP1*$^{-/-}$ cells, and PDS-treated 293T cells. The data represent mean ± S.E.M. (n = 3).

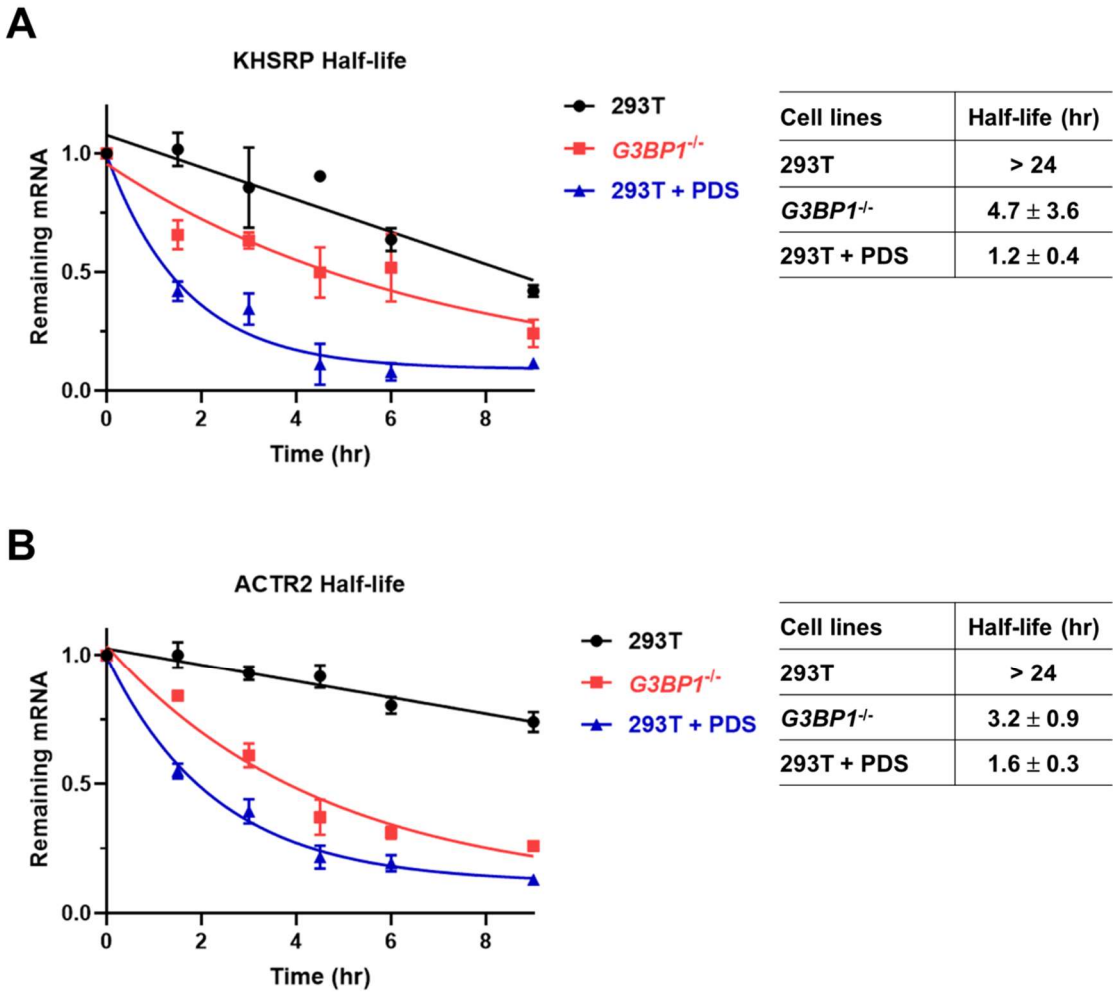

Cell lines	Half-life (hr)
293T	> 24
G3BP1$^{-/-}$	4.7 ± 3.6
293T + PDS	1.2 ± 0.4

Cell lines	Half-life (hr)
293T	> 24
G3BP1$^{-/-}$	3.2 ± 0.9
293T + PDS	1.6 ± 0.3

Figure S15. qPCR and Western blot results showing the mRNA and protein levels of *PITX1*, *KHSRP* and *ACTR2* genes in HeLa cells, G3BP1-depleted HeLa cells, HeLa cells without or with PDS treatment. (A-C) Relative mRNA and protein levels of the three genes in HeLa cells with or without PDS treatment. (D-F) Relative mRNA and protein levels of the three genes in HeLa cells and G3BP1-depleted HeLa cells. Error bars represent S.E.M. (n = 3). The *p* values were calculated by using unpaired, two-tailed Student's *t*-test. ns, $p > 0.05$; *, $0.01 \leq p < 0.05$; **, $0.001 \leq p < 0.01$; ***, $p < 0.001$.

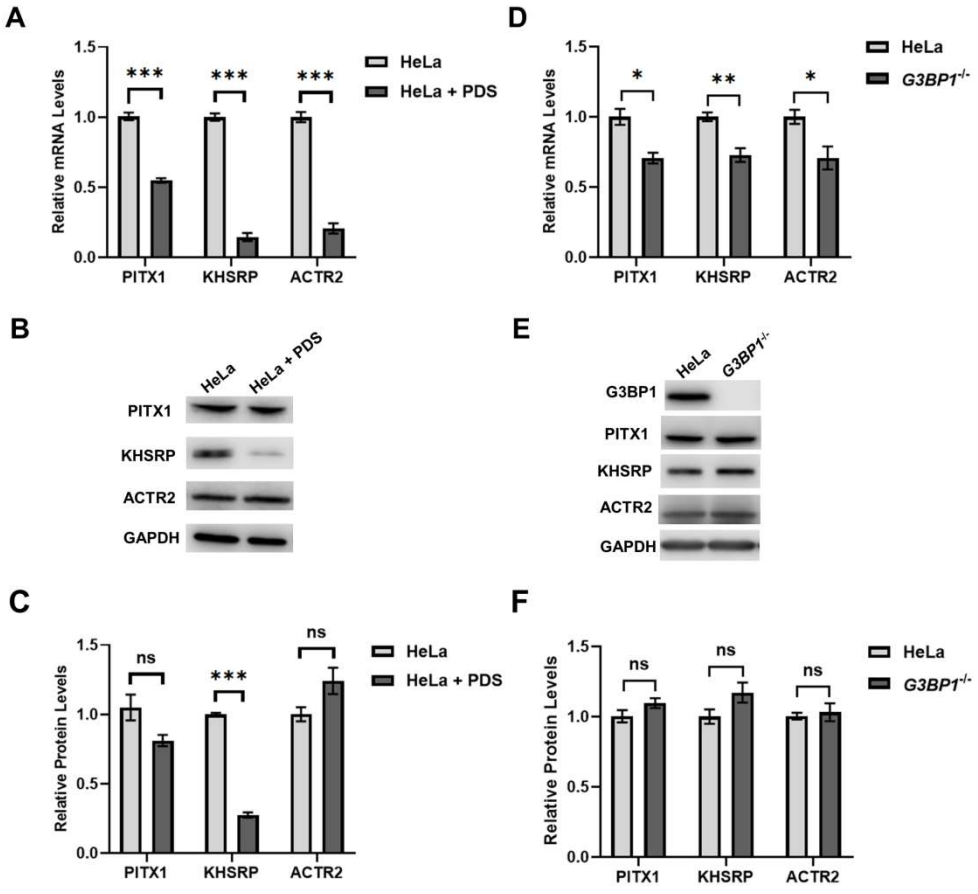

Figure S16. mRNA expression levels of PITX1 (A), KHSRP (B) and ACTR2 (C) in HepG2 and K562 cells. Base mean is the mean of normalized counts of replicates (n = 2). Standard deviations between replicates are unavailable in the datasets. *P* values are obtained from the datasets. ns, $p > 0.05$; *, $0.01 \leq p < 0.05$; ***, $p < 0.001$.

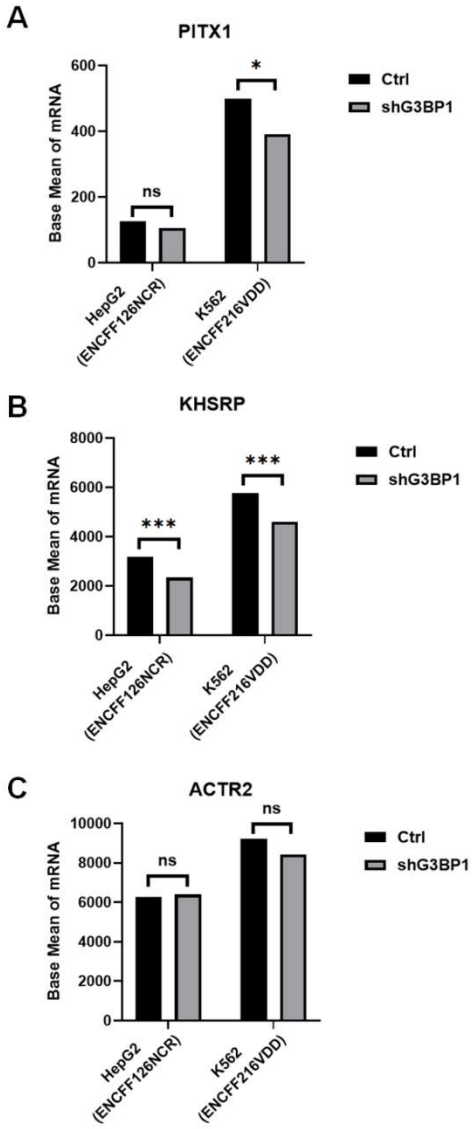

Figure S17. A comparison of human G3BP1, HNRNPA1 and HNRNPA2B1 proteins. (A) Schematic diagrams depicting the domain structures of the three proteins. IDR, intrinsically disordered region; RRM, RNA recognition motif; RG-rich, arginine-glycine rich. (B) Protein sequence alignment showing the sequence similarities among G3BP1 (Q13283), HNRNPA1 (P09651) and HNRNPA2B1 (P22626). Similar regions are highlighted in colors from gray to brown along with the increasing similarity.

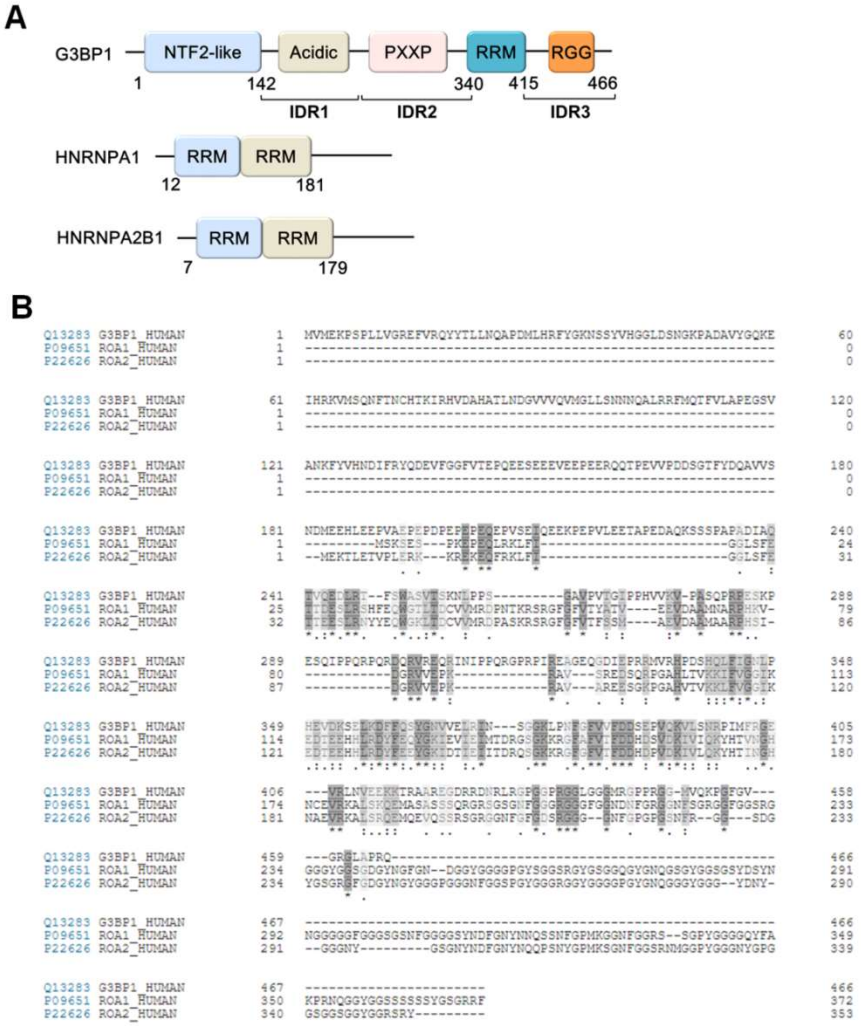

References:

1. Herdy, B., Mayer, C., Varshney, D., Marsico, G., Murat, P., Taylor, C., D'Santos, C., Tannahill, D. and Balasubramanian, S. (2018) Analysis of NRAS RNA G-quadruplex binding proteins reveals DDX3X as a novel interactor of cellular G-quadruplex containing transcripts. *Nucleic. Acids. Res.*, **46**, 11592-11604.
2. Kwok, C.K., Marsico, G., Sahakyan, A.B., Chambers, V.S. and Balasubramanian, S. (2016) rG4-seq reveals widespread formation of G-quadruplex structures in the human transcriptome. *Nat. Methods*, **13**, 841.
3. McRae, E.K.S., Booy, E.P., Moya-Torres, A., Ezzati, P., Stetefeld, J. and McKenna, S.A. (2017) Human DDX21 binds and unwinds RNA guanine quadruplexes. *Nucleic. Acids. Res.*, **45**, 6656-6668.
4. Ribeiro de Almeida, C., Dhir, S., Dhir, A., Moghaddam, A.E., Sattentau, Q., Meinhart, A. and Proudfoot, N.J. (2018) RNA Helicase DDX1 Converts RNA G-Quadruplex Structures into R-Loops to Promote IgH Class Switch Recombination. *Mol. Cell*, **70**, 650-662.e658.
5. Wu, G., Xing, Z., Tran, E.J. and Yang, D. (2019) DDX5 helicase resolves G-quadruplex and is involved in MYC gene transcriptional activation. *Proc. Natl. Acad. Sci.*, **116**, 20453-20461.
6. Murat, P., Marsico, G., Herdy, B., Ghanbarian, A., Portella, G. and Balasubramanian, S. (2018) RNA G-quadruplexes at upstream open reading frames cause DHX36- and DHX9-dependent translation of human mRNAs. *Genome Biol.*, **19**, 229.
7. Sexton, A.N. and Collins, K. (2011) The 5′ Guanosine Tracts of Human Telomerase RNA Are Recognized by the G-Quadruplex Binding Domain of the RNA Helicase DHX36 and Function To Increase RNA Accumulation. *Mol. Cell Biol.*, **31**, 736-743.
8. Wolfe, A.L., Singh, K., Zhong, Y., Drewe, P., Rajasekhar, V.K., Sanghvi, V.R., Mavrakis, K.J., Jiang, M., Roderick, J.E., Van der Meulen, J. *et al.* (2014) RNA G-quadruplexes cause eIF4A-dependent oncogene translation in cancer. *Nature*, **513**, 65.
9. Takahama, K., Kino, K., Arai, S., Kurokawa, R. and Oyoshi, T. (2011) Identification of Ewing's sarcoma protein as a G-quadruplex DNA- and RNA-binding protein. *Febs j*, **278**, 988-998.
10. Pietras, Z., Wojcik, M.A., Borowski, L.S., Szewczyk, M., Kulinski, T.M., Cysewski, D., Stepien, P.P., Dziembowski, A. and Szczesny, R.J. (2018) Dedicated surveillance mechanism controls G-quadruplex forming non-coding RNAs in human mitochondria. *Nat. Commun.*, **9**, 2558.
11. Herviou, P., Le Bras, M., Dumas, L., Hieblot, C., Gilhodes, J., Cioci, G., Hugnot, J.-P., Ameadan, A., Guillonneau, F., Dassi, E. *et al.* (2020) hnRNP H/F drive RNA G-quadruplex-mediated translation linked to genomic instability and therapy resistance in glioblastoma. *Nat. Commun.*, **11**, 2661.
12. Liu, X., Ishizuka, T., Bao, H.-L., Wada, K., Takeda, Y., Iida, K., Nagasawa, K., Yang, D. and Xu, Y. (2017) Structure-Dependent Binding of hnRNPA1 to Telomere RNA. *J. Am. Chem. Soc.*, **139**, 7533-7539.
13. Serikawa, T., Spanos, C., von Hacht, A., Budisa, N., Rappsilber, J. and Kurreck, J. (2018) Comprehensive identification of proteins binding to RNA G-quadruplex motifs in the 5′ UTR of tumor-associated mRNAs. *Biochimie*, **144**, 169-184.
14. Bian, W.-X., Xie, Y., Wang, X.-N., Xu, G.-H., Fu, B.-S., Li, S., Long, G., Zhou, X. and Zhang, X.-L. (2018) Binding of cellular nucleolin with the viral core RNA G-quadruplex structure suppresses HCV replication. *Nucleic. Acids. Res.*, **47**, 56-68.
15. Simko, E.A.J., Liu, H., Zhang, T., Velasquez, A., Teli, S., Haeusler, A.R. and Wang, J. (2020) G-quadruplexes offer a conserved structural motif for NONO recruitment to NEAT1 architectural lncRNA. *Nucleic. Acids. Res.*, **48**,

7421-7438.
16. Lyonnais, S., Tarrés-Solé, A., Rubio-Cosials, A., Cuppari, A., Brito, R., Jaumot, J., Gargallo, R., Vilaseca, M., Silva, C., Granzhan, A. *et al.* (2017) The human mitochondrial transcription factor A is a versatile G-quadruplex binding protein. *Sci. Rep.*, **7**, 43992.
17. von Hacht, A., Seifert, O., Menger, M., Schütze, T., Arora, A., Konthur, Z., Neubauer, P., Wagner, A., Weise, C. and Kurreck, J. (2014) Identification and characterization of RNA guanine-quadruplex binding proteins. *Nucleic. Acids. Res.*, **42**, 6630-6644.
18. Didiot, M.-C., Tian, Z., Schaeffer, C., Subramanian, M., Mandel, J.-L. and Moine, H. (2008) The G-quartet containing FMRP binding site in FMR1 mRNA is a potent exonic splicing enhancer. *Nucleic. Acids. Res.*, **36**, 4902-4912.
19. Majumder, M., House, R., Palanisamy, N., Qie, S., Day, T.A., Neskey, D., Diehl, J.A. and Palanisamy, V. (2016) RNA-Binding Protein FXR1 Regulates p21 and TERC RNA to Bypass p53-Mediated Cellular Senescence in OSCC. *PLoS genetics*, **12**, e1006306-e1006306.
20. Benhalevy, D., Gupta, S.K., Danan, C.H., Ghosal, S., Sun, H.-W., Kazemier, H.G., Paeschke, K., Hafner, M. and Juranek, S.A. (2017) The Human CCHC-type Zinc Finger Nucleic Acid-Binding Protein Binds G-Rich Elements in Target mRNA Coding Sequences and Promotes Translation. *Cell Rep.*, **18**, 2979-2990.
21. Thandapani, P., Song, J., Gandin, V., Cai, Y., Rouleau, S.G., Garant, J.M., Boisvert, F.M., Yu, Z., Perreault, J.P., Topisirovic, I. *et al.* (2015) Aven recognition of RNA G-quadruplexes regulates translation of the mixed lineage leukemia protooncogenes. *Elife*, **4**, 1-30.
22. Matsumoto, K., Okamoto, K., Okabe, S., Fujii, R., Ueda, K., Ohashi, K. and Seimiya, H. (2021) G-quadruplex-forming nucleic acids interact with splicing factor 3B subunit 2 and suppress innate immune gene expression. *Genes. Cells.*, **26**, 65-82.
23. Lyons, S.M., Kharel, P., Akiyama, Y., Ojha, S., Dave, D., Tsvetkov, V., Merrick, W., Ivanov, P. and Anderson, P. (2020) eIF4G has intrinsic G-quadruplex binding activity that is required for tiRNA function. *Nucleic. Acids. Res.*, **48**, 6223–6233.